Journal of ELECTRONIC MATERIALS, Vol. 49, No. 4, 2020
https://doi.org/10.1007/s11664-020-07975-5

Effect of ECAP Process and Subsequent Annealing on Microstructure and Properties of Cu-0.25Se-0.25Te Alloy

RUIJIE HUANG,[1] DACHUAN ZHU ,[1,2] XIN LIAO,[1] and QUN YAN[1]

1.—College of Materials Science and Engineering, Sichuan University, P.O. Box 610065, Chengdu, China. 2.—e-mail: zhudachuan@scu.edu.cn

Cu-0.25Se-0.25Te alloy has been melted in a vacuum induction furnace and then heat treated. Afterwards, equal-channel angular pressing (ECAP) and subsequent annealing were carried out on the obtained samples. The effects of the ECAP process and subsequent annealing on the microstructure and properties of the alloy have also been investigated by scanning electron microscopy, Vickers microhardness testing, and eddy-current conductivity measurements. The results suggest a morphological evolution of the grains during the ECAP process. The equiaxed grains of the heat-treated alloy initially developed into shapes elongated along the shearing plane, then a series of smaller streamlined strip-like grains appeared and were eventually crushed into fine and equiaxed grains with a size of about 5 μm after different numbers of ECAP passes (one, two, four, or eight), along with a deformed strain ε. Furthermore, the microhardness (HV) rose sharply from 68 N/mm^2 to 140 N/mm^2 and then climbed steadily to 169 N/mm^2 under the comprehensive effect of ε and the refinement of deformed grains. By contrast, the electrical conductivity decreased slowly from 96.2% international annealing copper standard (IACS) to 93.5% IACS. The microhardness and the electrical conductivity of the samples were found to vary contrarily with the change of annealing temperature and stabilized at 500°C. Notably, the electrical conductivity increased gradually, whereas the hardness of the alloys that were subject to a higher number of ECAP passes decreased remarkably with increasing annealing time at 300°C.

Key words: ECAP process, annealing, microstructures, Cu-Te-Se alloys

INTRODUCTION

Copper alloys are widely used in various electrical and electronic applications, e.g., as connectors, in integrated circuits, as contact wires for high-speed railways, etc.[1] With the rapid development of manufacturing in recent years, copper alloys with high strength and high conductivity have been explored to obtain good comprehensive properties.[2–4] However, addition of alloy elements (Cr, Zr, Mg, and Ag) would increase the defects in the Cu matrix, thus impairing the electrical conductivity.[5] To alleviate this problem, severe plastic deformation (SPD) techniques have been developed as an effective process to obtain ultrafine-grained (UFG) materials with superior mechanical properties and good electrical conductivity. To date, equal-channel angular pressing (ECAP), which allows the achievement of extremely large imposed strains through intensive simple shear in a bulk sample, is considered one of the most promising SPD processes to procure materials with high strength and high conductivity simultaneously.[6–8] In ECAP, significant grain refinement occurs together with dislocation hardening, resulting in radical changes in both the mechanical and electrical performance.[9] Several groups have investigated the microstructure and mechanical behavior of pure Cu,[10] Cu-Cr,[9–11] Cu-

(Received July 8, 2019; accepted January 24, 2020; published online February 5, 2020)

Cr-Zr,[6,12,13] Cu-Ni-Si,[8,14] and Cu-Mg-Ce[15] alloys after ECAP deformation, and their results suggest that the mean grain size decreased gradually, while the dislocation density multiplied as the number of ECAP passes was increased. The enhanced strength was attributed to grain refinement and high dislocation density deriving from large strain deformation, but the deformation strengthening contribution was greater than the fine-grain strengthening.[13,16] In previous studies, addition of Te or Se to the Cu matrix has been demonstrated to be beneficial for the reduction of impurity elements (O, Al, H, S, P, etc.) and amelioration of the microstructure.[17] The binary phase diagrams[18] of Cu-Te and Cu-Se alloys show that the solubility of Te and Se in pure Cu is very low, nearly zero at room temperature, with Te or Se being present as Cu_2Te or Cu_2Se, indicating that they would be of great benefit to enhance the alloy's strength without undermining its intrinsic high electrical conductivity. Zhu's group[17,19] studied the effects of the annealing temperature on the electrical conductivity and mechanical properties of Cu-Te alloys, and their results show that the tensile strength of copper alloys could be improved by adding Te to pure copper, while the electrical conductivity could reach 94% to 98% IACS. Jiao et al.[20] investigated the corrosion behavior of Cu-Se-Te alloys in 3.5% sodium chloride solution and found that adding a small amount of Te and Se could improve the corrosion resistance of pure copper. Therefore, Cu-Se-Te alloy is expected to show good comprehensive performance and combine high strength with high conductivity. To further improve the mechanical and electrical properties of Cu-Se-Te alloys, ECAP was chosen in this work as an effective measure. Accordingly, the aim of this study is to investigate the evolution of the microstructure of the Cu-Se-Te alloy during the ECAP process and the effect of ECAP on its mechanical properties and electrical conductivity. The thermal stability and subsequent annealing of the studied alloy are also discussed. Cu-Se-Te alloy is expected to be widely applied in contact wires, transformers, and other electric or electronic fields due to its high strength and high conductivity.

EXPERIMENTAL PROCEDURES

First, the required raw materials were weighed according to the designed ratio of the Cu-0.25Se-0.25Te (wt.%) alloy and then melted using a vacuum induction furnace under an argon protected atmosphere. Since both the melting and boiling points of selenium and tellurium are low (221°C and 685°C for Se, 449.5°C and 988°C for Te), they are easy to volatilize. To reduce the burning loss and consequently improve the utilization efficiency of the added alloy elements, both Se and Te elements were added as intermediate alloys (Cu-5Te, Cu-5Se) by the powder metallurgy method.

The detailed procedures for alloy melting were as follows: (1) A two-stage vacuum device including a mechanical pump and a diffusion pump was first used to achieve a vacuum degree in the melting furnace cavity below 10^{-1} Pa; (2) The cavity was then vacuumized after the remaining air had been discharged by high-purity argon (99.99%), after which argon was filled repeatedly for three times to reduce the influence of impurity elements in the atmosphere on the melting process of the alloy; (3) In the melting process of the alloy, the melting temperature was controlled by adjusting the current (power) and a magnetic stirring device was used to ensure the uniformity of the composition in each melting process. The actual composition of the investigated sample ingots was determined by x-ray fluorescence (XRF; ADVAN). The designed and measured contents of Se and Te are listed in Table I.

After being kept at 850°C for 4 h, the ingots were quenched and subsequently forged into copper plate with a thickness of 18 mm. Several cylindrical rods, with dimensions of Φ9.8 mm × 90 mm, were cut from the central copper plate, as shown in Fig. 1a. ECAP was conducted at room temperature using a die with an internal channel angle of Φ = 110° and an outer arc curvature of ψ = 20° at the intersection

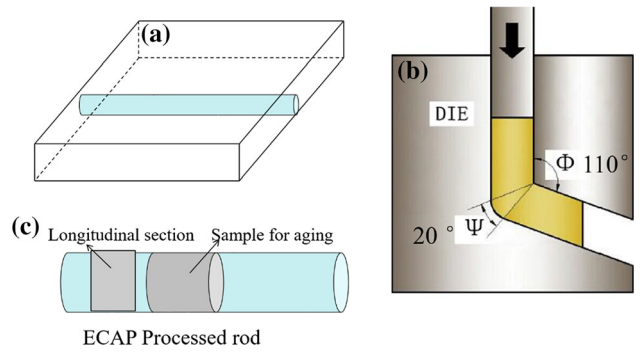

Fig. 1. Schematic illustration of (a) cutting of cylindrical rods for ECAP, (b) geometry of die used, and (c) position of samples for microstructure analysis and annealing in ECAP-processed rod.

Table I. Designed and measured contents of Te and Se (wt.%) for Cu-0.25Se-0.25Te alloy

Designed Se Content (wt.%)	Measured Se Content (wt.%)	Designed Te Content (wt.%)	Measured Te Content (wt.%)
0.25	0.149	0.25	0.243

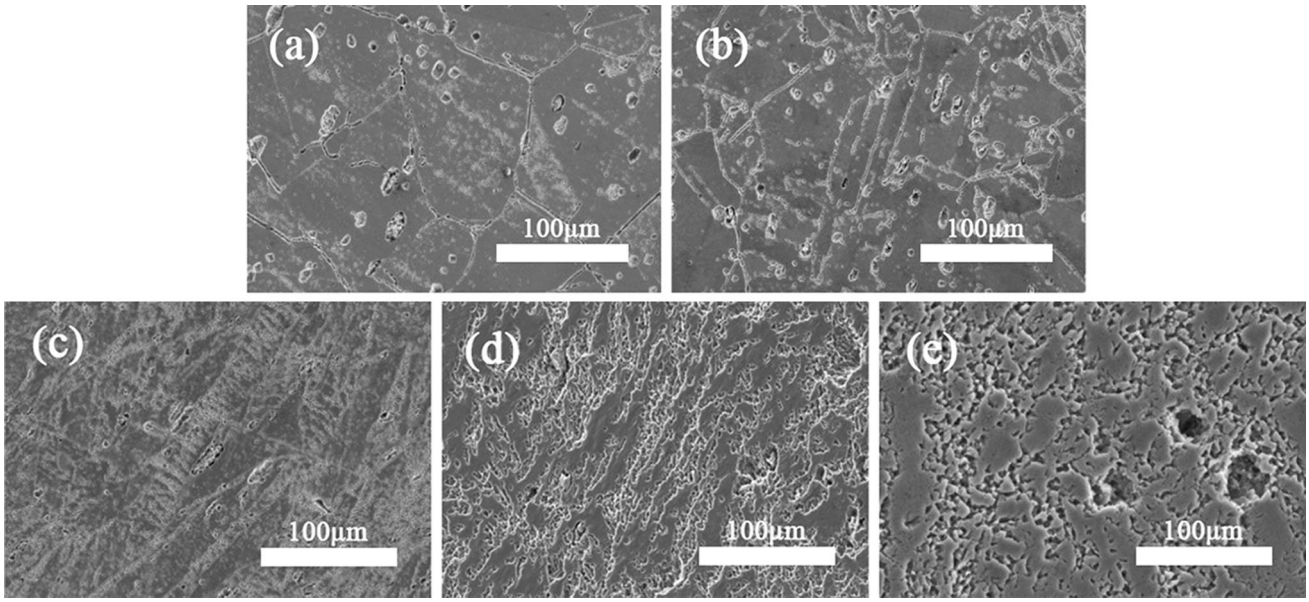

Fig. 2. SEM morphology of samples after different numbers of ECAP passes: (a) zero, (b) one, (c) two, (d) four, and (e) eight.

of two parts of the channel, as depicted in Fig. 1b. An imposed strain of ~ 0.5 was exerted in each separate pass using these angles. The billets were covered with MoS_2 powder as lubricant before extrusion, then the extrusion speed was controlled at 7 mm/s through a total number of one, two, four, and eight passes using a route in which each billet was rotated 90° around the pressing direction between each pass. Segalll and Iwahashi[21,22] investigated the effect of the internal channel angle Φ and outer arc curvature of ψ on the stress and corresponding strain under good lubrication due to the neglected friction:

$$\varepsilon = \left[\frac{2\cot\left(\frac{\phi}{2}+\frac{\psi}{2}\right)+\psi\mathrm{cosec}\left(\frac{\phi}{2}+\frac{\psi}{2}\right)}{\sqrt{3}}\right]. \qquad (1)$$

After ECAP processing, samples with dimensions of Φ9.8 mm × 10 mm were machined from the billets as shown in Fig. 1c, and annealed at 200°C, 300°C, 350°C, 400°C, 450°C, and 500°C for 1 h in a tube furnace with argon gas atmosphere. The microhardness was measured using a Vickers microhardness tester with a load of 1.98 N for 15 s at different locations. The electrical conductivity was measured by an eddy-current conductivity meter according to the international annealed copper standard (IACS). After that, the morphology of the samples was observed by scanning electron microscopy (SEM, JSM-5910 LV) at a 15-kV accelerating voltage. By contrast, backscattered electron (BSE) imaging and element composition measurements were carried out on the alloys by SEM (Apreo; Thermo Scientific) equipped with energy-dispersive x-ray spectroscopy (EDX, X-Max 80; Oxford; with Aztec software) at a 20-kV accelerating voltage.

RESULTS AND DISCUSSION

Effect of ECAP on Microstructure of Cu-0.25Se-0.25Te Alloy

Figure 2 presents the SEM morphology of the samples after different numbers of ECAP passes. Note that the number of passes had an obvious effect on the microstructure. Before ECAP, the microstructure of the initial material after heat treatment mainly consisted of undeformed and equiaxed grains with an average size of about 80 μm (Fig. 2a), along with some dispersed secondary phase. After the first pass of ECAP, many unevenly deformed grains with a length of about 50 μm and a width of about 20 μm were yielded under the shear force. After the second and fourth passes of extrusion, the grains were further elongated along the shearing plane, and a streamlined strip structure appeared. It is notable that the grain width after the fourth pass of extrusion was apparently smaller than that after the second pass. However, the strip-like grains were broken into fine and equiaxed grains with a size of about 5 μm when the number of ECAP passes reached eight. This evolution of the microstructure matches well with the three typical refinement stages of ECAP.[10]

To confirm the elemental distribution and composition of the secondary phases, backscattered electron (BSE) analysis combined with energy-dispersive x-ray spectroscopy (EDX) analysis was carried out in detail on the sample subjected to eight ECAP passes and annealing at 400°C. EDX mapping of Cu, Se, Te, and O in the annealed sample is depicted in Fig. 3, and the element composition of

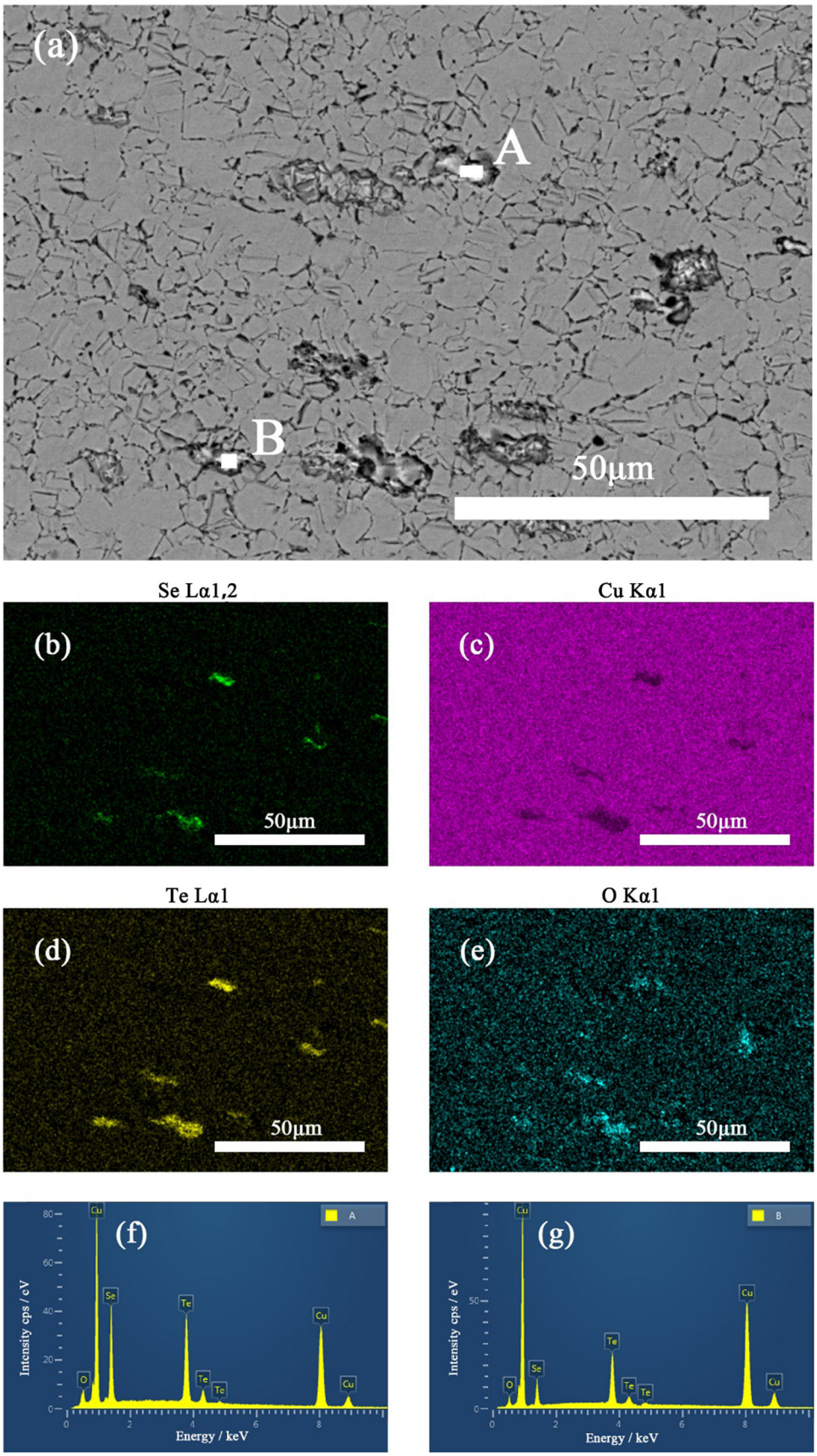

Fig. 3. BSE morphology (a); EDX mapping of Cu (b), Se (c), Te (d), and O (e); EDX spectra at points marked A (f) and B (g).

the second phases marked A and B is listed in Table II. It is deduced that Se and Te exist as the second phases at the same site, since both of them share some similar characteristics, such as their location in the same group of the Periodic Table and very low solubility in copper at room temperature.

Effect of ECAP on Microhardness and Electrical Conductivity

Figure 4 shows that increasing the number of ECAP passes improved the microhardness of the sample.

In particular, the microhardness (HV) was dramatically enhanced from 68 N/mm^2 to 140 N/mm^2 after the first pass. With continuation of the ECAP process, the microhardness (HV) increased gradually to 169 N/mm^2 due to the comprehensive effect of ε and refinement of deformed grains. By contrast, the electrical conductivity of the sample decreased slowly from 96.2% IACS to 93.5% IACS after eight passes. Firstly, in the process of ECAP extrusion, an additional ε forms along with a large number of dislocations, which is helpful to enhance the stress field and strain field in the crystal. Thus, the resistance to dislocation slip rises via the interaction of accumulated dislocations; i.e., the movement of dislocations is restrained under external stress.[21] Secondly, with increasing number of ECAP passes, the grains are refined. According to the Hall–Petch principle, Eq. 2 the finer the grains, the higher the hardness of the metal[6]:

$$\mathrm{HV} = \mathrm{HV}_0 + K_{\mathrm{HV}} d^{-1/2}, \tag{2}$$

where HV represents the hardness number of the material, HV_0 stands for the hardness number with infinite grains, K_{HV} refers to the hardening coefficient, and d is the average grain size.

Therefore, with increasing number of ECAP passes, the strength or hardness of the material increases, since the deformed grains become smaller along with an increase in the dislocations and ε. However, the presence of vacancies, dislocations, or crystal boundaries, which act as point, linear, and planar defects in the crystal, respectively, reduces the electrical conductivity, since all defects increase the scattering of mobile electrons in metals. van Beuren defines the dependence of the electrical resistivity on defects as

$$\Delta\rho = C\varepsilon^n, \tag{3}$$

where $\Delta\rho$ represents the increment of the electrical resistivity, C is a constant related to the purity of the metal, ε refers to the degree of plastic deformation, and n varies from 0 to 2.

Although the additional ε increases with increasing number of ECAP passes, which can be evaluated using Eq. 1, fortunately, the electrical resistivity rises only slightly by 2% to 6% even under severe deformation, and the resulting decrease of the electrical conductivity is confined to within 3% IACS.

Table II. Elemental composition of second phases in sample

Element	A at.%	B at.%
Cu K	53.77	75.88
Se L	21.71	7.88
Te L	16.87	10.51
O K	7.65	5.73
Total	100.00	100.00

Sample subjected to eight ECAP passes and annealing at 400°C.

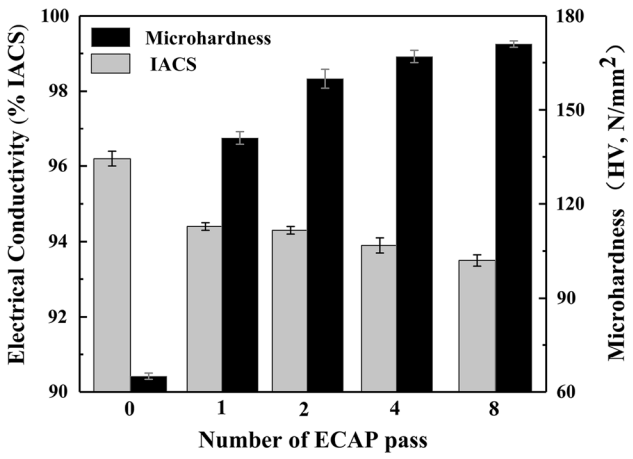

Fig. 4. Microhardness and electrical conductivity of samples after different numbers of ECAP passes.

Effects of Annealing Temperature on Microstructure and Properties of the Alloy

Figure 5 displays the SEM morphology of the alloy samples after annealing for 1 h at different temperatures. Note that deformed grains still exist in the case of low annealing temperature below 200°C. However, when the annealing temperature is increased to 300°C, the deformed grains are replaced by small equiaxed grains, indicative of recrystallization. Even coarse grains with twin wafers can be found after annealing at temperature of 500°C. Compared with the traditional annealing temperature of deformed copper alloys of 400°C, it is verified that severe deformation (eight passes) can decrease the recrystallization temperature.

Figure 6 depicts the effect of the annealing temperature on the electrical conductivity and hardness of the samples after different numbers of ECAP passes. For the sample not treated by mechanical deformation processing (zero passes), the biggest change in microstructure is that Se and Te

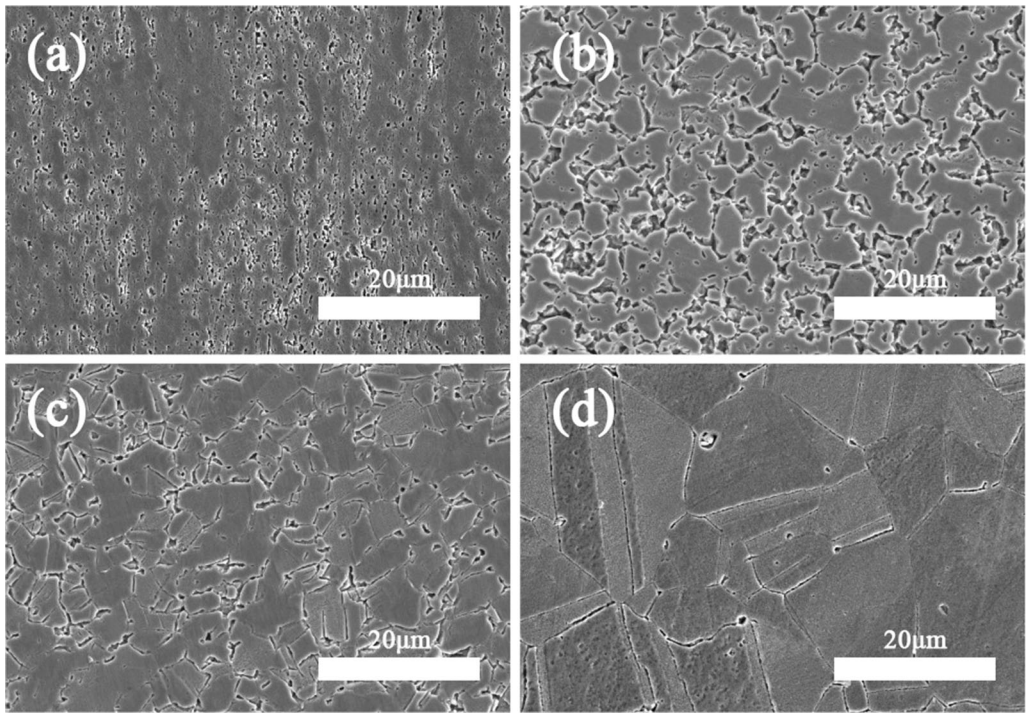

Fig. 5. SEM morphology of alloy samples (subjected to eight ECAP passes) after annealing for 1 h at (a) 200°C, (b) 300°C, (c) 400°C, and (d) 500°C.

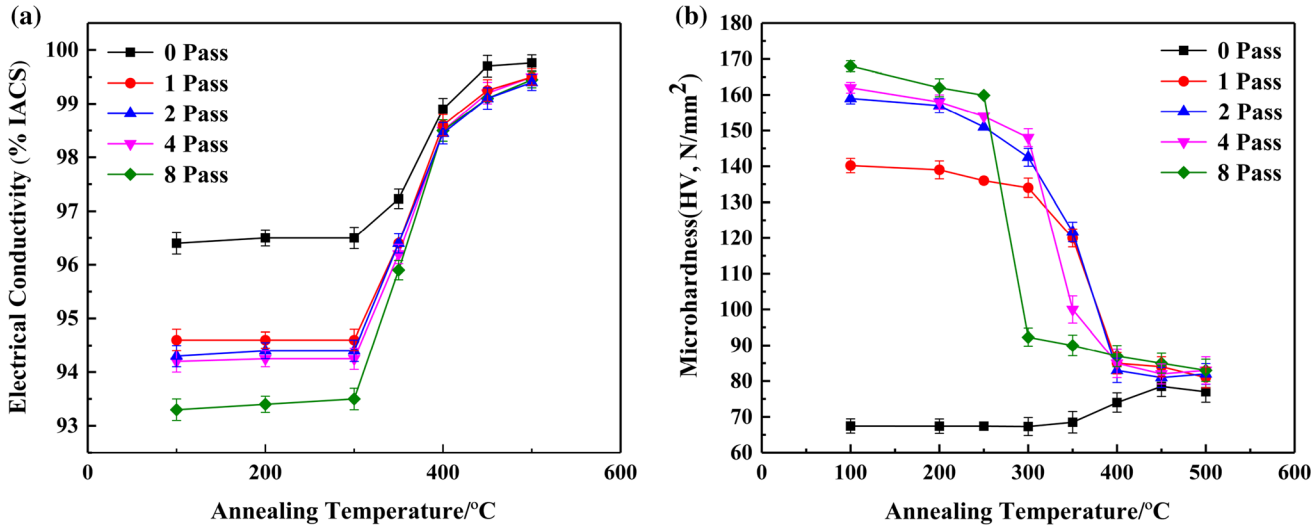

Fig. 6. Effect of annealing temperature (for 1 h) on the (a) electrical conductivity and (b) microhardness of samples subjected to different numbers of ECAP passes.

precipitate as the second phase $Cu_2(Se,Te)$, thus the conductivity still rises. However, this kind of precipitation has two opposite effects on the hardness: one is that the solid-solution strengthening effect is weakened, whereas the precipitation strengthening can be enhanced, thus the final hardness remains slightly increased. By contrast, for the samples subjected to different numbers of ECAP passes, it was found that the electrical conductivity remained practically constant below 300°C then rose rapidly, while the microhardness decreased with increasing annealing temperature. In addition, it can also be seen that the electrical conductivity and microhardness of the samples subjected to a higher number of ECAP passes changed more remarkably, even though the final values reached a relatively stable level when the annealing temperature was 500°C. This phenomenon can be explained as follows: With increasing annealing temperature, the deformed grains tend to recover, recrystallize, and

grow, as shown in Fig. 4, resulting in a decrease, and even elimination, of the deformation strain ε and the dislocations present in the ECAP sample, as well as a corresponding reduction of the grain boundaries. Meanwhile, with increasing numbers of ECAP passes, the temperature at which recovery and recrystallization occur reduced, since severe deformation always enhances the metastability of microstructure with higher distortional strain energy.

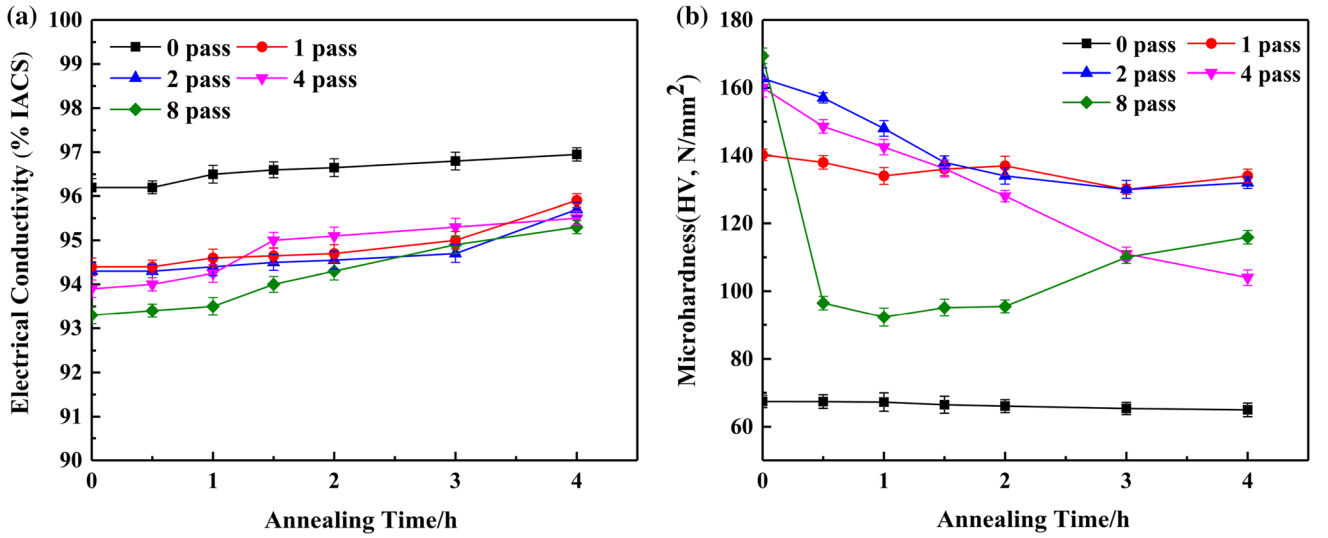

Fig. 7. Effect of annealing time on (a) electrical conductivity and (b) microhardness of alloys annealed at 300°C.

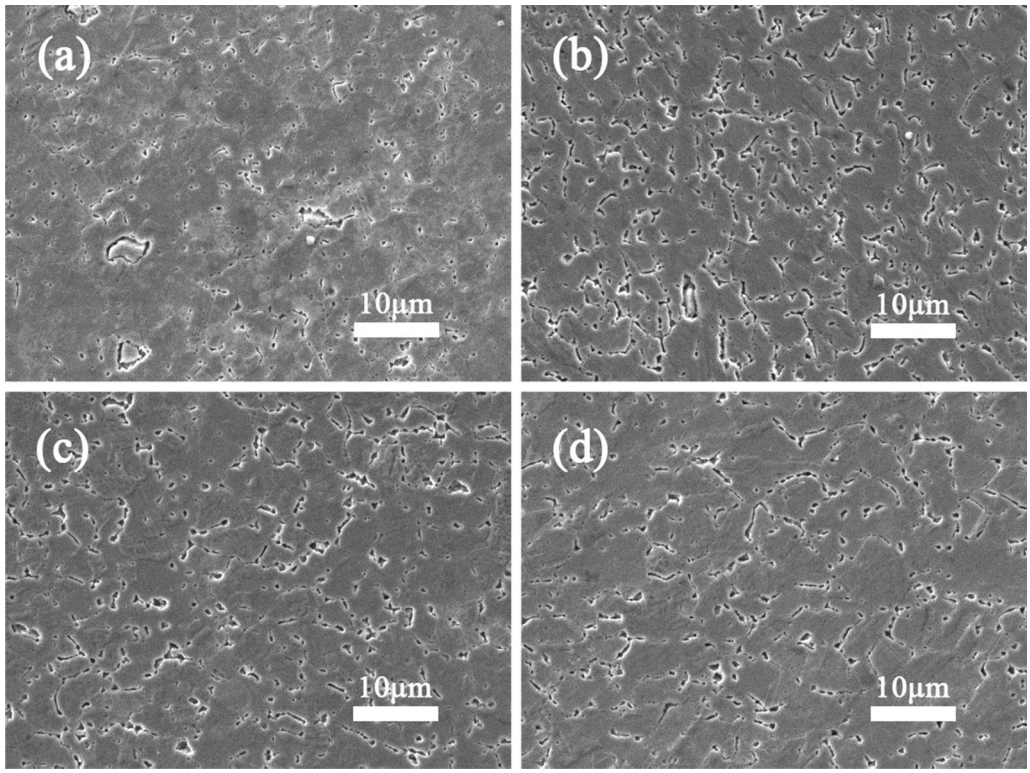

Fig. 8. SEM morphology of alloy after eight ECAP passes and annealing at 300°C for (a) 0.5 h, (b) 1 h, (c) 2 h, and (d) 4 h.

Effects of Annealing Time on Microstructure and Properties of the Alloy

Figures 7 and 8 exhibit the effect of the annealing time at 300°C on the electrical conductivity, microhardness, and microstructure of the alloys. With prolongation of the annealing time, the electrical conductivity gradually increased, since the deformed alloys only recovered partially at the relatively low annealing temperature of 300°C. By contrast, the hardness of the alloys decreased slightly. In particular, for the alloys subjected to eight passes of ECAP, the hardness (HV) initially decreased obviously from 169 N/mm^2 to 96 N/mm^2, but increased with continuing annealing, which may result from the fact that recovery, recrystallization, and grain growth, along with precipitation of the second phase, occurred successively.

CONCLUSIONS

The following conclusions can be drawn from the investigation of the effect of the ECAP process and subsequent annealing on the microstructure and properties of Cu-0.25Se-0.25Te alloy:

1. After different numbers of ECAP passes (one, two, four, and eight), the grains of the heat-treated alloy evolved from equiaxed to a shape elongated along the shearing plane, then a smaller streamlined strip structure appeared, and eventually, the stripped grains were broken into fine and equiaxed grains with a size of about 5 μm; ε after each ECAP pass can be predicted.
2. With increasing number of ECAP passes, the microhardness rose obviously from 68 HV to 140 HV at the beginning, then climbed gradually to 169 HV under the comprehensive effect of ε and refinement of deformed grains. By contrast, the electrical conductivity decreased slowly from 96.2% IACS to 93.5% IACS.
3. After annealing at different temperatures for 1 h, the microhardness of the samples decreased while the electrical conductivity rose obviously, and finally both the microhardness and electrical conductivity reached stable values at annealing temperature of 500°C.
4. As the annealing time at 300°C was prolonged, the electrical conductivity gradually increased; by contrast, the hardness of the alloys subjected to a higher number of ECAP passes decreased remarkably.

ACKNOWLEDGMENTS

This work is supported by Sichuan Science and Technology Program Grant No. 2019YFG0228 and the Fundamental Research Funds for the Central Universities.

REFERENCES

1. Y.X. Ye, X.Y. Yang, J. Wang, X.K. Zhang, Z.L. Zhang, and T. Sakai, *J. Alloys Compd.* 615, 249 (2014).
2. R. Mahmudi, A. Karsaz, A. Akbari-Fakhrabadi, and A.R. Geranmayeh, *Mater. Sci. Eng. A* 527, 2702 (2010).
3. Sh Raygan, H. Ehsanian Mofrad, M. Pourabdoli, and F.K. Ahadi, *J. Mater. Process. Technol.* 211, 1810 (2011).
4. F.L. Wang, Y.P. Li, K. Wakoh, Y. Koizumi, and A. Chiba, *Mater. Des.* 61, 70 (2014).
5. Kazunari Maki, Yuki Ito, Hirotaka Matsunaga, and Hiroyuki Mori, *Scr. Mater.* 68, 777 (2013).
6. A. Vinogradov, V. Patlan, Y. Suzuki, K. Kitagawa, and V.I. Kopylov, *Acta Mater.* 50, 1639 (2002).
7. Khadidja Abib, Jairo Alberto Munoz Balanos, Baya Alili, and Djamel Bradai, *Mater. Charact.* 112, 252 (2016).
8. F.H. Larbi, H. Azzeddine, T. Baudin, M.-H. Mathon, F. Brisset, A.-L. Helbert, M. Kawasaki, D. Bradai, and T.G. Langdon, *J. Alloys Compd.* 638, 88 (2015).
9. A. Vinogradov, T. Ishida, K. Kitagawa, and V. Kopylov, *Acta Mater.* 53, 2181 (2005).
10. J. Xu, J.W. Li, D.B. Shan, and B. Guo, *Mater. Sci. Eng. A* 664, 114 (2016).
11. K.X. Wei, W. Wei, F. Wang, Q.B. Du, I.V. Alexandrov, and J. Hu, *Mater. Sci. Eng. A* 528, 1478 (2011).
12. G. Purcek, H. Yanar, M. Demirtas, Y. Alemdag, D.V. Shangina, and S.V. Dobatkin, *Mater. Sci. Eng. A* 649, 114 (2016).
13. R. Mishnev, I. Shakhova, A. Belyakov, and R. Kaibyshev, *Mater. Sci. Eng. A* 629, 29 (2015).
14. A.Y. Khereddine, F.H. Larbi, M. Kawasaki, T. Baudin, D. Bradai, and T.G. Langdon, *Mater. Sci. Eng. A* 576, 149 (2013).
15. G. Yang, Z. Li, Y. Yuan, and Q. Lei, *J. Alloys Compd.* 640, 347 (2015).
16. O. Nejadseyfi, A. Shokuhfar, and V. Moodi, *Trans. Nonferrous Met. Soc. China* 25, 2571 (2015).
17. D.C. Zhu, K. Tang, M.Z. Song, and M.J. Tu, *Trans. Nonferrous Met. Soc. China* 16, 459 (2006).
18. Y. Jueqi (edit and transform), Phase Diagrams of Binary Alloys. Shanghai: Science and Technology Press (1987).
19. D.C. Zhu, W. Huang, M.Z. Song, and M.J. Tu, *J. Wuhan Univ. Technol. Mater.* 22, 88 (2007).
20. L. Jiao, M. Li, T. Zeng, and D.C. Zhu, *J. Mater. Eng. Perform.* 24, 4333 (2015).
21. V.M. Segal, *Mater. Sci. Eng. A* 197, 157 (1995).
22. Y. Iwahashi, J. Wang, and Z. Horita, *Scr. Mater.* 35, 143 (1996).